Selective inhibitor of endosomal trafficking pathways exploited by multiple toxins and viruses

Eugene J. Gillespie[a], Chi-Lee C. Ho[a], Kavitha Balaji[b], Daniel L. Clemens[c], Gang Deng[d], Yao E. Wang[a], Heidi J. Elsaesser[a], Batcha Tamilselvam[e], Amandeep Gargi[e], Shandee D. Dixon[a], Bryan France[a,f], Brian T. Chamberlain[d,f], Steven R. Blanke[e], Genhong Cheng[a], Juan Carlos de la Torre[g], David G. Brooks[a], Michael E. Jung[d,f], John Colicelli[b], Robert Damoiseaux[f], and Kenneth A. Bradley[a,f,1]

[a]Department of Microbiology, Immunology, and Molecular Genetics, University of California, Los Angeles, CA 90095; [b]Department of Biological Chemistry, David Geffen School of Medicine, University of California, Los Angeles, CA 90095; [c]Department of Medicine, Division of Infectious Diseases, David Geffen School of Medicine, University of California, Los Angeles, CA 90095; [d]Department of Chemistry and Biochemistry, University of California, Los Angeles, CA 90095; [e]Department of Microbiology, Institute for Genomic Biology, University of Illinois at Urbana–Champaign, Champaign, IL 61801; [f]California NanoSystems Institute, University of California, Los Angeles, CA 90095; and [g]Department of Immunology and Microbial Science, The Scripps Research Institute, La Jolla, CA 92037

Pathogenic microorganisms and toxins have evolved a variety of mechanisms to gain access to the host-cell cytosol and thereby exert virulent effects upon the host. One common mechanism of cellular entry requires trafficking to an acidified endosome, which promotes translocation across the host membrane. To identify small-molecule inhibitors that block this process, a library of 30,000 small molecules was screened for inhibitors of anthrax lethal toxin. Here we report that 4-bromobenzaldehyde N-(2,6-dimethylphenyl)semi-carbazone, the most active compound identified in the screen, inhibits intoxication by lethal toxin and blocks the entry of multiple other acid-dependent bacterial toxins and viruses into mammalian cells. This compound, which we named EGA, also delays lysosomal targeting and degradation of the EGF receptor, indicating that it targets host-membrane trafficking. In contrast, EGA does not block endosomal recycling of transferrin, retrograde trafficking of ricin, phagolysosomal trafficking, or phagosome permeabilization by Francisella tularensis. Furthermore, EGA does not neutralize acidic organelles, demonstrating that its mechanism of action is distinct from pH-raising agents such as ammonium chloride and bafilomycin A1. EGA is a powerful tool for the study of membrane trafficking and represents a class of host-targeted compounds for therapeutic development to treat infectious disease.

The success of a broad array of microbial pathogens depends on their ability to gain entry into and/or transport proteins into the cytosol of host cells. Intracellular-acting bacterial toxins have evolved to take advantage of numerous host-mediated entry mechanisms (1), making these toxins ideal tools for studying endocytosis and vesicular trafficking. Indeed, the use of bacterial toxins has contributed to many key discoveries, including membrane recycling, clathrin-independent endocytosis, and retrograde transport (2). Compounds that inhibit entry of ricin, Shiga toxin, and *Pseudomonas aeruginosa* exotoxin A (ExoA) into host cells have been identified (3–5). These small molecules exhibit varied mechanisms of action, including blockade of retrograde toxin trafficking at the early endosome–trans Golgi network (TGN) junction, morphological disruption of the Golgi apparatus, and inhibition of the toxin active site. Small molecules that disrupt toxin binding, entry, trafficking, and host response can serve not only as probes to dissect such eukaryotic cellular pathways, but also are potential therapeutics for infectious and genetic diseases.

Bacillus anthracis, the causative agent of the disease anthrax, secretes binary toxins that enter host cells and disrupt physiological processes. Lethal factor (LF) is a Zn^{2+}-dependent metalloprotease that cleaves mitogen-activated protein kinase kinases (MAPKKs) 1–4, 6, and 7 (6, 7) and Nlrp1b (8–10) and reproduces many pathologies of anthrax when injected into laboratory animals (11, 12). The cellular entry of LF is dependent on a cell-binding and translocation subunit known as protective antigen (PA). PA is an 83-kDa protein that is cleaved by host proteases into 63- and 20-kDa fragments, allowing oligomerization of the toxin into a prepore (13). The PA oligomer can then bind up to four monomers of LF, forming a holotoxin complex (14, 15). Two cellular toxin receptors, TEM8 and CMG2, mediate toxin binding and endocytic uptake (16, 17). Acidification of the lumen of the late endosome drives a conformational change in the prepore, resulting in insertion into the endosomal membrane and translocation of LF into the cytosol (18–20). Alternatively, LF may be translocated to the interior of intraluminal vesicles and transported to the late endosome via multivesicular bodies in a process dependent on COPI and ALIX (21). The vesicular membranes then fuse with the limiting endosomal membrane and thereby deliver LF to the cytosol (21).

Despite substantial effort to define binding and entry mechanisms used by lethal toxin (LT), much is still unknown about how it, and indeed many other toxins and viruses, gain access to the host cytosol. To address this, we performed a high-throughput screen to identify small molecules that block cellular entry of LT. Here, we report the identification and characterization of a compound that blocks trafficking of various toxins and viruses to acidified endosomes.

Results

High-Throughput Screen Identifies Potent Anthrax Toxin Inhibitor. To identify inhibitors of toxin entry, we used a cellular intoxication

Significance

Bacterial and viral infections are a significant public health burden. To corrupt normal host cellular functions, many bacterial toxins and all viruses must gain entry to host cells, a process that exploits the host's own cellular machinery. In this study, we use high-throughput technologies to screen for chemical inhibitors of bacterial toxin and viral entry. We report the discovery of a small molecule that inhibits several viruses and bacterial toxins. In addition to the therapeutic potential, this compound represents a powerful probe for dissecting the mechanisms of mammalian membrane trafficking processes.

assay using an immortalized macrophage cell line that undergoes a rapid cell death known as pyroptosis in response to anthrax LT. Pyroptosis is a proinflammatory, caspase-1–dependent cell death that occurs in response to LT in macrophages and dendritic cells encoding certain alleles of the inflammasome gene *Nlrp1b* (22). This rapid cytolytic response occurs within 2–3 h of toxin addition and provides a convenient assay for toxin entry. A total of 30,000 small molecules from a commercially available compound library were screened for their ability to inhibit LT-mediated cytotoxicity. Hits were defined based on percentage of survival relative to untreated controls. All compounds that yielded survival greater than 7% (~0.1% hit rate) were selected for initial revalidation. Thirty-seven initial hits were picked from the source library, assembled onto a single master plate, and retested for protection in the LT macrophage cytotoxicity assay. Compounds that increased survival at least three SDs above controls treated with LT and vehicle were considered verified. Thirty-two compounds exhibited activity in validation assays, whereas five failed to reconfirm. Of the 32 confirmed hits, fresh powder stocks were ordered for 8 compounds, including the 5 that displayed the highest level of protection from LT. Six of these yielded calculable IC$_{50}$ values in the macrophage cytotoxicity assay (Fig. 1*A* and Fig. S1*A*), and the other two compounds showed no activity.

The most potent of the validated compounds, 4-bromobenzaldehyde *N*-(2,6-dimethylphenyl)semicarbazone, which we called EGA, rescued viability up to 100% of unintoxicated controls with an IC$_{50}$ of 1.7 μM (Fig. 1*A* and *B* and Fig. S1 *A* and *B*). EGA could be added up to 15 min after LT and still protect cells from killing (Fig. 1*C*), suggesting that this compound acts after toxin binding to host cells but at a step early in intoxication.
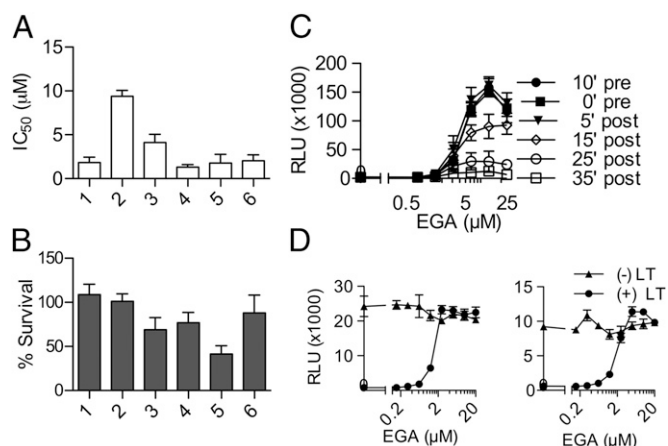

Fig. 1. High-throughput screen reveals small-molecule inhibitors of LT. (*A* and *B*) Six hits from a high-throughput screen of 30,000 compounds were further characterized for their ability to protect RAW264.7 cells from LT. (*A*) IC$_{50}$ and (*B*) maximal cell protection values were calculated from three independent experiments performed in triplicate (Fig. S1 *A* and *B*). Compound names and ChemBridge ID are the following: 1, EGA [4-bromobenzaldehyde *N*-(2,6-dimethylphenyl)semicarbazone] (5319257); 2, 1-(2,6-dimethyl-1-piperidinyl)-3-[(2-isopropyl-5-methylcyclohexyl)oxy]-2-propanol hydrochloride (5807685); 3, 1-(3,6-dichloro-9H-carbazol-9-yl)-3-(dimethylamino)-2-propanol (5236848); 4, 4-fluoro-*N*′-[1-(2-pyridinyl)ethylidene]benzohydrazide (5325699); 5, 17-{[(2-hydroxyethyl)amino]methyl}androstan-17-ol (5709157); 6, 1,1′-(1,4-phenylene)bis[3-(2-pyridinyl)-2-propen-1-one] (5276688). (*C*) EGA was added to RAW264.7 cells at various times before or after the addition of LT. Cell survival was measured at 24 h post-toxin addition via ATPlite assay, with relative luminescence units (RLU) correlating with increased survival. Data represent average values of triplicate samples ±SD from a representative experiment. (*D*) BMDMs from two independent mice bearing LT-sensitive alleles of *Nlrp1b* were treated with a dose titration of EGA followed by LT or media for 3 h, after which viability was measured as above. Averages and SDs were calculated independently from technical triplicates for each mouse.

To determine if the effect of EGA extended beyond established cell lines, primary bone marrow-derived macrophages (BMDMs) from mice with an LT-sensitive *Nlrp1b* transgene were intoxicated in the presence or absence of EGA. Whereas BMDMs treated with DMSO vehicle were killed efficiently by LT, BMDMs treated with EGA were protected (Fig. 1*D*).

NMR and liquid chromatography–mass spectrometry (LC-MS) analysis confirmed purity and structure of commercial EGA (Fig. S2 *A* and *B*), reducing the possibility that the activity of EGA is due to a contaminant from its synthesis and/or from a breakdown product. Resynthesis of EGA yielded similar activity as that obtained from the commercial source (Fig. S2*C*), further validating the identity of the compound. As an initial investigation of the structure–activity relationship, a series of related compounds from Chembridge was assayed. Interestingly, none of the commercially available EGA analogs were active (Fig. 2 and Fig. S3). These compounds revealed critical roles for four-position substitution on the benzaldehyde, as well as 2,6 substitutions on the aniline ring. Furthermore, the semicarbazone linker appeared to contribute to compound activity.

EGA Inhibits Cytosolic Entry of LF. To identify the step at which EGA blocks LT-mediated cytotoxicity, processes involved in cellular entry and pyroptosis were assessed in the presence and absence of this compound. Caspase-1 activation, which occurs late in LT intoxication, can be monitored using a fluorescent probe, FLICA, which specifically binds to active caspase-1. Although vehicle-treated controls showed high levels of caspase-1 activity upon LT treatment, active caspase-1 was not detected in EGA-treated cells challenged with LT (Fig. 3*A*). This result indicates that EGA blocks intoxication upstream of caspase-1 activation.

Activation of caspase-1 by LT is a late step in pyroptosis and depends on the activity of the proteasome, lysosomal membrane permeabilization, and LF catalytic activity (10, 23–25). To determine if EGA blocks a step upstream of LF proteolysis of MAPKKs, we assessed cleavage of MEK2 by immunoblot. Whereas LT cleaved MEK2 in vehicle-treated controls in both RAW264.7 cells and toxin-sensitive BMDMs, treatment with EGA completely abrogated this effect (Fig. 3*B*). EGA-treated cells were also found to be resistant to treatment with PA + LFnDTA, a chimeric protein that delivers the catalytic diphtheria toxin A chain to the cytosol in a PA-dependent fashion (Fig. S4) (26). Because LF induces pyroptosis and diphtheria toxin induces apoptosis due to inhibition of protein synthesis, inhibitors blocking both could affect some shared mechanism of internalization. These data, combined with the caspase-1 and MEK2 data, strongly suggest that EGA interferes with PA-mediated toxin entry.

In order for LF to reach the cytosol, PA$_{83}$ must be proteolytically activated to PA$_{63}$, oligomerize into a prepore form, bind LF, and traffic to a low-pH endosome where it undergoes an acid-dependent conformational change from prepore to pore (18–20). Host-cell binding, proteolytic processing, and pore formation were monitored by immunoblot in the presence and absence of EGA. Specifically, the pore form of PA resulting from exposure to acidified endosomes is resistant to dissociation by SDS and runs as an oligomer on SDS/PAGE, whereas immature prepores formed by PA$_{63}$ are dissociated by SDS and run as monomers (20). EGA completely inhibited formation of the SDS-resistant oligomer but did not block binding of PA$_{83}$ to cells or proteolytic processing to generate PA$_{63}$ (Fig. 3*C*). The effective dose range for EGA inhibition of oligomer formation (Fig. 3*D*) closely mirrored the IC$_{50}$ in the toxicity assay (Fig. 1). These results indicate that EGA blocks intoxication at a step downstream of toxin assembly on the host-cell surface but upstream of trafficking to acidified endosomes.
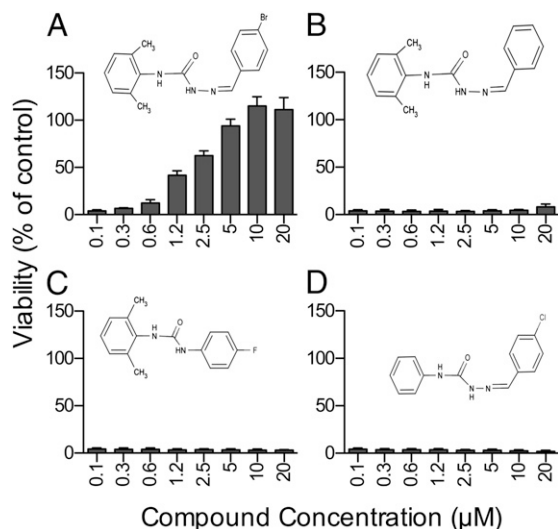
Fig. 2. Structure–activity relationship for EGA. EGA and commercially available structural analogs were tested for ability to inhibit LT-mediated cytotoxicity. RAW264.7 cells were seeded at 2×10^3 cells/well on 384-well plates and the following day were incubated with indicated doses of (*A*) EGA [4-bromobenzaldehyde *N*-(2,6-dimethylphenyl)semicarbazone] (5319257), (*B*) Benzaldehyde *N*-(2,6-dimethylphenyl)semicarbazone (5319438), (*C*) *N*-(2,6-dimethylphenyl)-N′-(4-fluorophenyl)urea (9062150), and (*D*) 4-chlorobenzaldehyde *N*-phenylsemicarbazone (5191420) for 1 h, followed by intoxication with 500 ng/mL PA + 500 ng/mL LF. Cell viability was measured 24 h later as in Fig. 1. Average values ±SD from technical replicates in a single representative experiment shown.

Impact of EGA on Endosomal Trafficking. Neutralization of acidic compartments by lysosomotropic agents like NH_4Cl is a well-established technique for blocking anthrax toxin entry (27, 28). The observed block to pore formation raised the possibility that EGA functions by neutralizing low-pH–dependent steps in the endocytic pathway. To address this possibility, Lysotracker Red

DND-99 was used to probe acidic compartments in the cell. Lysotracker is a red-fluorescent dye used for tracking acidic organelles in the cell, and neutralization of these compartments can be visualized as a loss in punctate, red-fluorescent structures. Ammonium chloride and bafilomycin A1, a specific inhibitor of vacuolar-type H^+-ATPases, markedly decreased cell-associated Lysotracker Red fluorescence (Fig. 3*E*). EGA, on the other hand, did not reduce Lysotracker Red signal at concentrations that fully protected cells from LT. These results suggest that EGA blocks the ability of PA to access acidified endosomes but does not function by neutralizing acidic compartments.

We next considered whether EGA-mediated inhibition of endosomal trafficking extended beyond anthrax toxin–receptor interactions by examining trafficking of the epidermal growth factor receptor (EGFR). HeLa cells were treated with epidermal growth factor (EGF), and the stability of EGFR was measured by immunoblotting. At the high dose of EGF used in these experiments (100 ng/mL), EGFR is trafficked to lysosomes and degraded (29). Lysosomal degradation of EGFR depends on the acidic luminal pH, and lysosomotropic agents such as NH_4Cl inhibit EGF-induced receptor degradation (Fig. 4*A*) (30). Unlike NH_4Cl, EGA treatment did not stabilize EGFR at 60 min. EGA treatment did slow degradation somewhat, however, with significantly less EGFR degraded at 30 min post-EGF stimulation ($P < 0.05$) (Fig. 4*B*). This suggested that EGA inhibits trafficking, but that this inhibition can be overcome by excess ligand stimulation over longer periods of time. To test this, we determined the ability of EGA to block lysosomal degradation induced by a lower dose of EGF (20 ng/mL). We used fluorescently labeled EGF to visualize EGFR trafficking and degradation microscopically. EGA treatment stabilized the EGF signal at 60 min, compared with vehicle (DMSO)-treated controls (Fig. 4*C*). Notably, EGA treatment also resulted in EGF being retained in enlarged endosomes that stained positive for the early endosome marker EEA1 (Fig. 4*C*). These findings indicated that EGA does not block initial binding or endocytic uptake from the plasma membrane, but does inhibit trafficking from early to late endosomes.
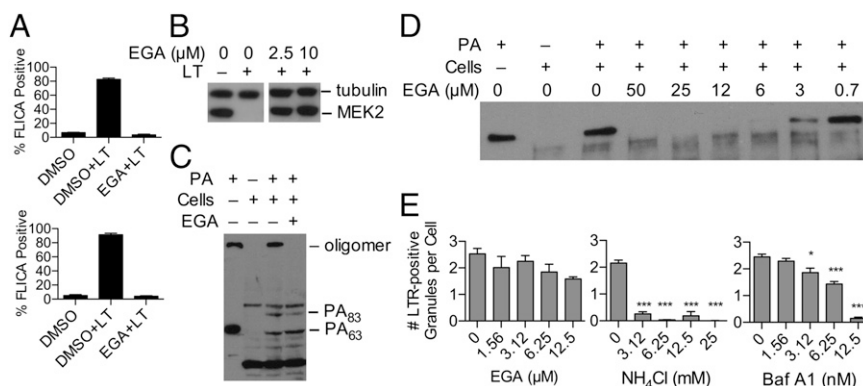

Fig. 3. EGA inhibits cellular entry of LF. (*A*) EGA inhibits LT-mediated caspase-1 activation. BMDMs (2×10^4/well) were seeded on clear-bottom 384-well plates, allowed to adhere overnight, and then incubated with 20 μM EGA or DMSO for 1 h before addition of 500 ng/mL PA + 500 ng/mL LF for 2 h. FLICA was added for a further 1 h and then cells were stained with Hoechst 33342 and analyzed by automated fluorescence microscopy. Percentage of cells with active caspase-1, as measured by FLICA, was calculated from all cells in each well. Average values of three wells per condition are graphed with SE. Results graphed are average values of three technical replicates ±SD from BMDMs derived from two independent mice. (*B*) EGA inhibits LT-mediated cleavage of MEK-2. RAW264.7 cells were incubated with EGA or DMSO for 1 h before addition of vehicle control or 231 ng/mL PA + 33 ng/mL LF for 2.5 h. Cells were lysed and analyzed via immunoblotting with a MEK-2–specific antibody. Tubulin was used as a loading control. (*C*) EGA inhibits PA pore formation. RAW264.7 cells were incubated with 25 μM EGA for 1 h before addition of 400 ng/mL PA for an additional 1 h. Cells were lysed with 1% Nonidet P-40 buffer and analyzed by immunoblotting with a PA-specific antibody. (*D*) EGA inhibits PA pore formation in a dose-dependent manner. RAW264.7 cells were incubated with a dose titration of EGA for 1 h before addition of 400 ng/mL PA for an additional 1 h. Cells were lysed and analyzed as in *C*. (*E*) EGA does not neutralize acidic vessicles. HeLa cells were treated with compounds or vehicle control for 25 min at 37 °C before addition of Lysotracker Red (LTR) and Hoechst 33342 for a further 10 min. Cells were imaged by automated fluorescent microscopy, and images were scored for number of LTR-positive structures per cell. Results shown in *B–E* are representative of at least three independent experiments.
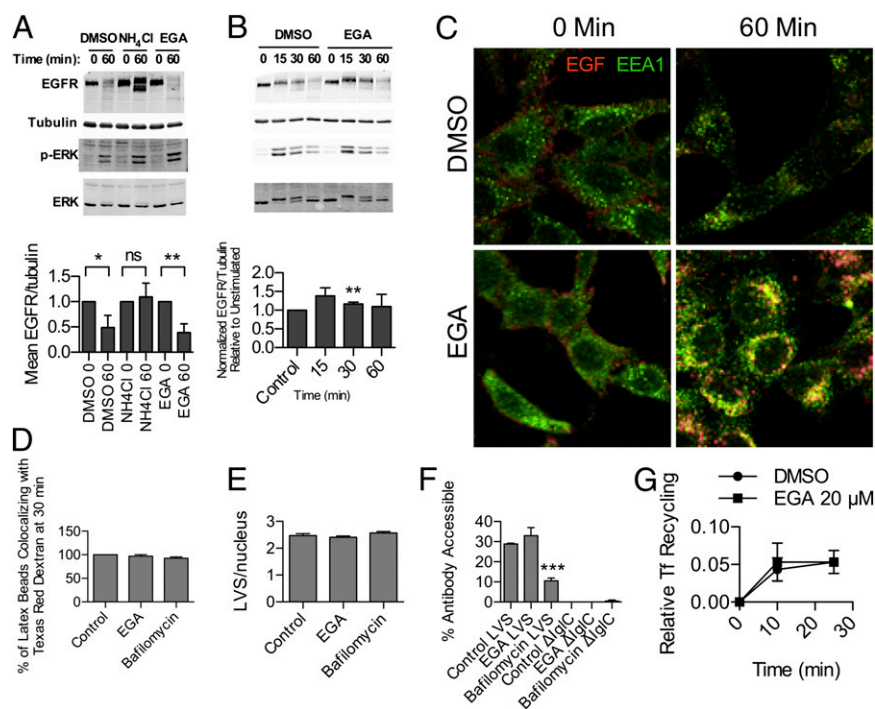
Fig. 4. EGA specifically disrupts trafficking from early to late endosomes. (*A* and *B*) EGA slows, but does not block degradation of EGFR induced by high-dose EGF. HeLa cells were treated with compounds or vehicle control and then stimulated with 100 ng/mL EGF for indicated times. Cell lysates were analyzed by immunoblotting with indicated antibodies. EGFR signal was normalized to tubulin, and the average values from at least three independent experiments are shown ±SD. (*C*) EGA treatment results in EGF retention in EEA1+ endosomes. HeLa cells were treated with EGA or vehicle and then stimulated with 20 ng/mL fluorescently labeled EGF (red). Cells were then stained for EEA1 (green), and images were acquired by confocal microscopy. (*D*) EGA does not block fusion of latex bead phagosomes with Texas Red-Dextran–labeled lysosomes. Lysosomal compartments of human THP-1 monocytic cells were prelabeled by overnight incubation with Texas Red Dextran, treated for 1 h with 20 μM EGA or 250 nM bafilomycin A1, and incubated with 1 μm polystyrene beads. After 3 h incubation at 37 °C, cells were fixed, and colocalization of endocytosed Texas Red Dextran with phagocytosed polystyrene beads was measured. Data represent average values of at least 40 particles ±SE and are representative of two independent experiments. (*E*) EGA does not block phagocytic uptake of *F. tularensis*. THP-1 cells were incubated with compounds for 1 h followed by infection with the LVS strain of *F. tularensis* for 3 h. Cells were fixed and stained for bacteria and host nuclei. Results represent average values of at least 400 cells for each of two replicates ±SE and are representative of two independent experiments. (*F*) EGA does not block *F. tularensis* permeabilization of its phagosome. THP-1 cells were treated with compounds followed by addition of either LVS or an LVS mutant (ΔIglC) that cannot escape from the host phagosome. After 3 h, cells were permeabilized with digitonin and stained with antibody against *F. tularensis*. Percentage of bacteria accessible to antibody was determined by examination under phase-contrast and fluorescence microscopy. Results represent the average values of at least 400 cells on each of two replicates ±SE and are representative of two independent experiments. Bafilomycin A1 treatment, but not EGA treatment, markedly inhibited permeabilization of the *F. tularensis* phagosome (***$P < 0.001$). (*G*) EGA does not inhibit transferrin receptor recycling to the plasma membrane. HeLa cells were incubated with 20 μg/mL fluorescently labeled Tf at 4 °C for binding and then chased with fresh media at 37 °C. The relative levels of Tf recycling for EGA- and vehicle-treated cells were assessed at 10 and 25 min post-chase.

To determine whether other vesicular trafficking events were blocked by EGA, we tested the effect of this compound on phagocytosis and phagolysosomal trafficking. Neither EGA nor bafilomycin A1 inhibited fusion of latex bead-containing phagosomes with lysosomes that had been prelabeled with Texas-red dextran in human monocytic cells (Fig. 4*D*). To extend this experiment to bacterial pathogens, we asked whether EGA affects phagocytosis and trafficking of *Franciscella tularensis*, a Gram-negative pathogen that causes the potentially deadly disease tularemia in humans. Neither EGA nor bafilomycin A1 blocked phagocytic uptake of a live vaccine strain (LVS) of *F. tularensis* (Fig. 4*E*). Furthermore, EGA had no effect on *F. tularensis* permeabilizatoin of its phagosome as determined by accessibility of LVS to antibody staining in digitonin-treated cells (Fig. 4*F*) (31–33). In contrast, escape was inhibited by bafilomycin A1 in the time frame of this assay. Therefore, although EGA blocks trafficking of PA to acidified endosomes, this compound does not inhibit phagocytic uptake, trafficking of endosomes to phagocytic compartments, or phagosome maturation required for escape of *F. tularensis*.

To further elucidate the specificity of EGA, we assessed the effect of this compound on endosome recycling using fluorescently

labeled transferrin (Tf), which binds the Tf receptor (TFRC). Like the anthrax toxin receptor (ANTXR), TFRC is taken up by clathrin-mediated endocytosis upon binding its ligand. TFRC releases its iron cargo into the lumen of early endosomes, and then the iron-free Tf-TFRC complex is recycled back to the cell surface through a Rab11-dependent process (34). EGA had no effect on the amount of Tf recycled back to the surface of cells by 10 and 25 min post-binding (Fig. 4*G*), indicating that this compound does not affect endosomal uptake or recycling.

EGA Inhibits Entry of pH-Dependent Bacterial Toxins. Several bacterial toxins and viruses are known to share similar entry requirements with LT, including trafficking to an acidified endosome. Two such toxins, *P. aeruginosa* ExoA and diphtheria toxin (DT) affect cells by ADP ribosylating EF-2, thereby halting protein synthesis (35–38). In contrast, the plant toxin ricin does not require trafficking to acidified endosomes. Ricin is an *N*-glycosylase that modifies the 28S rRNA of the eukaryotic ribosome and thereby inhibits translation. Unlike the three previously mentioned toxins, ricin is transported in a retrograde fashion to the endoplasmic reticulum (ER) and retrotranslocated into the cytosol by the host ER-associated degradation pathway (2). EGA effectively pro-

tected HeLa cells from DT and ExoA (Fig. 5A). In contrast, cytotoxicity mediated by ricin was not blocked by EGA (Fig. 5B). These data support the hypothesis that EGA inhibits the entry of toxins that require acidified endosomes.

Based on the observation that EGA blocks entry of toxins that require trafficking to acidified endosomes, we next asked whether we could use this inhibitor to characterize entry pathways for toxins that are less well studied. Cytolethal distending toxins (CDTs) are produced by multiple human pathogens, where they promote invasiveness and/or persistence (39). CDTs are tripartite AB toxins consisting of a single catalytic domain, CdtB, and two cell-binding domains, CdtA and CdtC. CdtB is ultimately trafficked to the host nucleus where it acts as a DNase, triggering DNA damage response, cell-cycle arrest, and apoptosis (40). Studies on CDT from *Haemophilus ducreyi* (Hd-CDT) indicate that this toxin, unlike ricin, traffics through acidified endosomes in addition to retrograde trafficking through Golgi and ER (41, 42). However, CDTs from other pathogens have distinct host factors for binding and entry (42–44), indicating that entry pathways used by various CDTs may be idiosyncratic to each. To test this, we determined the ability of EGA to inhibit intoxication by Hd-CDT as well as CDT derived from *Escherichia coli* (Ec-CDT). As expected, EGA inhibited Hd-CDT–mediated cytotoxicity (Fig. 5C). Interestingly, EGA did not inhibit intoxication by Ec-CDT (Fig. 5C), supporting the recent conclusion that these related toxins enter cells through distinct trafficking pathways (42). Consistent with the EGA-mediated accumulation of EGF in EEA1-positive compartments, Hd-CDT, but not Ec-CDT, was found to accumulate in enlarged vesicles that were EEA1-positive (Fig. 5D). These data, along with the lack of inhibition of phagocytosis and recycling, support the model that EGA targets a specific subset of vesicular trafficking pathways.

EGA Inhibits Entry of pH-Dependent Viruses. Upon ascertaining that EGA protects cells from several bacterial toxins, we hypothesized that EGA might also be able to inhibit viral entry. Influenza A virus, lymphocytic choriomeningitis virus (LCMV), and vesicular stomatitis virus (VSV), among others, require low pH for membrane fusion and infection of host cells (45–47). Distinct from these, amphotropic murine leukemia virus (A-MLV) and Nipah virus (NiV) both enter the cell in a pH-independent fashion (48, 49).

To test EGA-mediated inhibition of viral entry, we compared transduction by lentiviral vectors pseudotyped with NiV- and VSV-envelope glycoproteins in a cell culture model. The lentiviral genome used encodes green fluorescent protein (GFP), and successful transduction of the host cell results in expression of GFP in the cytosol. EGA effectively inhibited infection of HeLa cells by the low-pH–dependent VSV-pseudotyped lentivirus (Fig. 6A), but did not inhibit infection of cells by the pH-independent NiV-pseudotyped lentivirus (Fig. 6B).

The finding that EGA inhibits infection by VSV envelope glycoprotein (VSV-G)–pseudotyped lentiviruses encouraged us to assess its activity on infection by other viruses. We asked whether EGA could inhibit infection by A-MLV as well as by two human pathogens, LCMV and influenza. As expected, infection by A-MLV was not inhibited by EGA, as determined by GFP expression (Fig. 6C). As a control, we found that the same MLV core was neutralized when pseudotyped with VSV-G (Fig. 6D). LCMV is a rodent-borne virus that causes meningitis and encephalitis in humans and the prototypical member of the Arenaviridae, a family of viruses responsible for severe hemorrhagic fevers in humans. To determine if EGA affected LCMV multiplication, Vero cells were infected with serial dilutions of a recombinant GFP-expressing LCMV (Armstrong strain) (50). EGA decreased the total number of cells infected at 2 d after infection as determined by GFP
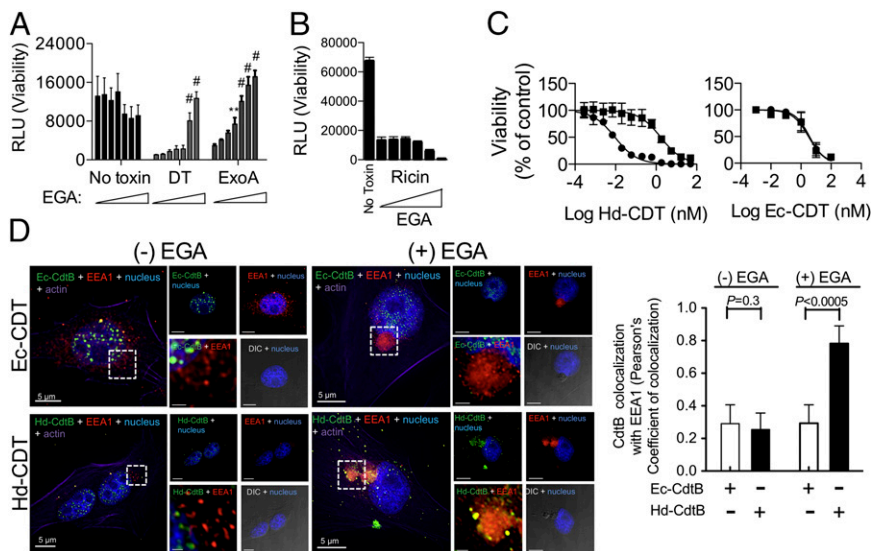

Fig. 5. EGA inhibits entry of low pH-dependent toxins. (A and B) EGA inhibits toxins that transit through acidic endosomes. HeLa cells were incubated with twofold dilutions of EGA for 1 h at 37 °C and then challenged with (A) DT at a concentration of 5 ng/mL, ExoA at 100 ng/mL, or (B) ricin at 5 ng/mL. EGA was titrated from 0.8 to 25 μM on DT- and ExoA-treated cells and from 1.6 to 25 μM on ricin-treated cells. Cells were incubated for 48 h and viability was assessed using ATPlite. Average relative luminescence unit (RLU) values of triplicate values from representative experiment were graphed ±SE. (C) EGA inhibits cytotoxicity induced by Hd-CDT but not Ec-CDT. CHO-pgsA745 cells were pretreated with 12.5 μM EGA (squares) or vehicle (circles) for 1 h and then treated with Hd-CDT or Ec-CDT. Cell viability was measured 96 h later by ATPlite. Data represent average values from three independent experiments performed in triplicate ±SD. (D) EGA traps Hd-CDT in enlarged EEA1-positive vesicles. HeLa cells were preincubated for 30 min in the absence or presence of EGA (20 μM) at 37 °C and further incubated with 100 nM of either Ec-CDT or Hd-CDT at 4 °C. After 30 min, cells were washed once with PBS, further incubated at 37 °C ± EGA (20 μM) for 60 min, and imaged by fluorescence microscopy. Images are representative of those collected from three independent experiments. (Right) Pearson's correlation coefficient for Ec-CdtB or Hd-CdtB colocalized with EEA1 from ~30 cells from each group over three independent experiments are rendered as a bar graph ±SD. Statistical significance was calculated for differences in the Pearson's correlation coefficient between cell populations incubated in the presence or absence of EGA.
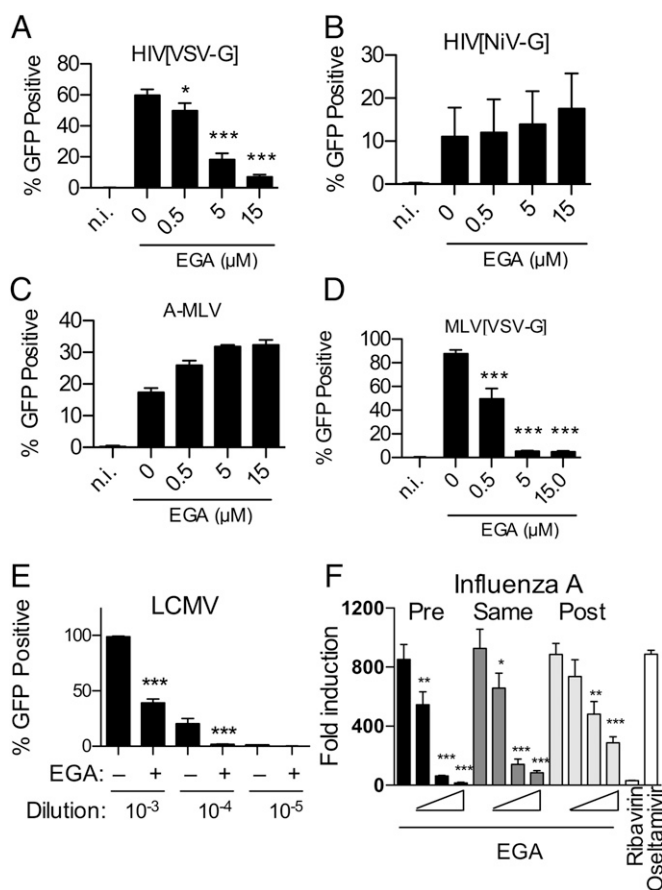
Fig. 6. EGA inhibits entry of low pH-dependent viruses. (*A* and *B*) EGA inhibits transduction by lentiviral particles pseudotyped with (*A*) VSV-G but not (*B*) NiV envelope proteins. (*C* and *D*) EGA does not inhibit infection by (*C*) A-MLV, but does inhibit transduction by (*D*) MLV particles pseudotyped with VSV-G. (*A–D*) HeLa cells were incubated with indicated dose of EGA for 1 h and then challenged with GFP-encoding viral particles for 2 d, followed by quantification of GFP expression by flow cytometry. Cells that were not infected (n.i.) did not express GFP. (*E*) Vero cells were incubated with 20 μM EGA for 1 h and then challenged with a GFP-encoding variant of the Arm-strong strain of LCMV at three dilutions as shown. Two days later, cells were fixed and analyzed by flow cytometery. (*A–E*) Average percentage of GFP-expressing cells from three independent experiments shown ±SD. (*F*) HeLa cells transfected with a Flu gLuc reporter were incubated with EGA (0.5, 5, or 15 μM) 1 h pre, simultaneously, or 1 h post-challenge with influenza A/WSN/33. The following day, luciferase activity was measured and normalized to uninfected controls. Average fold luciferase induction from three independent experiments is shown ±SD.

expression (Fig. 6*E*). Next, we investigated the effect of EGA on infection by the A/WSN/33 strain of influenza virus. Both LCMV and influenza virus are single-stranded, enveloped RNA viruses, but influenza virus belongs to the Orthomyxoviridae family rather than the Arenaviridae. To assess the effect of EGA on influenza virus infection, HeLa cells were transfected with a luciferase reporter responsive to the influenza polymerase complex. This assay can determine if infection by influenza virus is inhibited at any step up to the translation of viral proteins. Ribavirin and oseltamivir were used as controls. Ribavirin, an antiviral drug that blocks viral RNA synthesis, inhibits influenza and arenavirus infections and is the only licensed drug for treatment of arenavirus infection (51). Oseltamivir is a neuraminidase inhibitor that blocks influenza viral budding downstream of reporter activation (52). As expected, ribavirin effectively blocked reporter activation when added 1 h post-

infection, whereas oseltamivir exhibited no protection. EGA completely inhibited infection when added 1 h before or simultaneously with virus and even exhibited partial protection when added 1 h post-infection (Fig. 6*F*). Although EGA and ribavirin are active against both LCMV and influenza, their differential kinetics, along with the known mechanism of action of ribavirin, suggest that EGA targets a different process in the viral life cycle (53, 54).

In total, these data show that EGA inhibits cellular infection by multiple viruses, including two medically relevant human pathogens, influenza virus and LCMV. On the other hand, EGA did not block infection by NiV or A-MLV, indicating that it is a specific inhibitor of a subset of viruses that traffic to acidified endosomes.

Discussion

Here we report the use of high-throughput screening to identify a small molecule, EGA, that blocks cellular entry of bacterial toxins and viruses that require trafficking to acidified endosomes. This high-throughput screen leveraged the rapid cytolysis caused by LT in a subset of monocyte-derived cells from certain inbred strains of rodents. However, Nlrp1b-dependent cytolysis is a host-mediated protective response to LT rather than a mechanism of virulence (55). As such, it is necessary to carefully define the utility of the macrophage cytotoxicity assay and clarify the range of processes that could be affected. Inhibitors that act downstream of LF delivery to the cytosol would be most useful in investigating mechanisms of inflammasome activation, although they would not be predicted to be therapeutically relevant for anthrax. On the other hand, probing processes required for PA-mediated toxin entry is predicted to yield agents with therapeutic potential. A subset of the probes that block PA-mediated internalization are likely to interfere more generally with host endocytic processes, which, as described here, may expand their therapeutic relevance to other bacterial toxins and viruses and make them valuable chemical probes for studying host vesicular trafficking.

Indeed, despite the importance of endosomal trafficking in a myriad of cellular events, there is currently a dearth of chemical probes to study these processes. Dynamin-and clathrin-dependent events are blocked by dynasore and pitstop-1 and -2, respectively (56, 57). Arf1-dependent trafficking between ER and Golgi is blocked by Brefeldin-A (58). Finally, high-throughput screening for inhibitors of retrograde-trafficking toxins has resulted in identification of a small number of probes with unknown cellular targets (3, 5). Currently, investigation into the role of numerous other trafficking events relies on inhibitors that target trafficking indirectly, such as lysosomotropic drugs (i.e., bafilomycin A1, NH_4Cl, chloroquine, ionomycin, nigericin, monensin, etc.) or compounds that target multiple cellular processes in addition to blocking trafficking such as kinase inhibitors (i.e., staurosporine, calphostin C, genistein), phosphatase inhibitors (i.e., okadaic acid, orthovanadate), actin and microtubule inhibitors (i.e., jasplakinolide, latrunculin A, nocodazole, taxol), the HSP90 inhibitor geldanamycin (59), and cholesterol depletion (i.e., cyclodextrins, nystatin) (60). More specific inhibition of host proteins involved in trafficking can sometimes be achieved by overexpression of dominant negative or constitutively active versions of host proteins, i.e., Rab GTPases or RNAi-mediated knockdown. Although powerful, these approaches are limited to cells that are readily transfectable and are susceptible to compensatory mechanisms that may arise over the longer time course required to establish heterologous expression or knockdown.

The specific cellular target of EGA is currently unknown, but data presented here strongly suggest that the mechanism of action is through inhibition of trafficking between early and late endosomes. The requirement for low pH found in late endosomes is a characteristic shared by toxins, viruses, and natural receptor/li-

gand pairs such as EGFR/EGF, which were blocked by EGA. Many of the known inhibitors of LT target this step by directly neutralizing endosomal pH (27, 28). However, EGA does not block acidification of endosomes as determined by Lysotracker red staining (Fig. 4 *A* and *B*). Furthermore, EGA treatment caused an accumulation of EGF and Hd-CDT in enlarged endosomes that were positive for the early endosome marker EEA1 (Figs. 4*C* and 5*C*). Generation of enlarged EEA1-positive vesicles is also seen when overexpressing a constitutively active form of Rab5 (61), consistent with maturation/trafficking between early and late endosomes as a target for EGA. Importantly, recycling endocytosis of TFRC, phagocytosis of polystyrene beads and live bacteria, and retrograde trafficking of ricin and Ec-CDT were all unaffected by EGA, indicating that this compound inhibits a specific trafficking event.

EGA is an aryl semicarabazone with structural similarity to compounds developed as anticonvulsive agents (62). The molecular target for anticonvulsive semicarbazones is unknown, but these drugs are thought to function by altering levels of the neurotransmitter GABA (62). It is possible that EGA shares a molecular target with anticonvulsive aryl semicarbazones, although the high degree of specificity observed in initial structure-activity relationship studies suggests that EGA may have unique target(s) (Fig. 2). Indeed, one of the most active anticonvulsive aryl semicarbazones, benzaldehyde *N*-(2,6-dimethylphenyl)semicarbazone (62), showed almost no activity against LT (Fig. 2). EGA is a potent small molecule for studying vesicular trafficking and represents a class of host-targeted inhibitors that may be developed as therapeutics to treat bacterial and viral disease.

Materials and Methods

Reagents. PA and LF were expressed and purified as described previously (55). LF$_N$DTA (a fusion of the amino terminus of LF with the diphtheria toxin A chain) was a gift from Jeremy Mogridge (University of Toronto). DT and *Pseudomonas* ExoA were purchased from List Biological Laboratories. Ricin, bafilomycin A1, and anti–β-tubulin antibody were purchased from Sigma Aldrich. Anti-PA rabbit serum was obtained from Covance. Anti–MEK-2 N-terminal antibody was purchased from Santa Cruz Biotechnology. Horseradish peroxidase (HRP)-conjugated anti-rabbit antibody was obtained from Invitrogen. HRP-conjugated anti-mouse antibody was purchased from AnaSpec. The compound library was from ChemBridge (DiverSet E) and made available through the Molecular Screening Shared Resource at the University of California at Los Angeles. Working stock solutions of compounds were 1-mM compound in DMSO and were stored in sealed 384-well plates at room temperature in dessicated chambers.

High-Throughput Screen. RAW 264.7 macrophages were cultured in complete growth medium consisting of DMEM containing 10% (vol/vol) FBS, 100 U/mL penicillin, 100 μg/mL streptomycin, 6.25 mM Hepes, and 1× GlutaMAX-1 supplement (Invitrogen). Two thousand cells were added to each well of the 384-well white polystyrene plates (Matrix) in a volume of 40 μL per well. The cells were allowed to grow overnight at 37 °C, 5% CO$_2$. The following day, 0.5 μL of 1-mM compound in DMSO was pin-transferred onto cells with a Biomek FX (Beckman Coulter) and custom 500-nL pin transfer tool (V&P Scientific) to achieve a 12-μM final concentration of each compound per well. Cells were incubated with compound for 1 h at 37 °C, 5% CO$_2$, and then challenged with LT by adding 15 μL of 1.4×10^{-9} M LF and 1.0×10^{-8} M PA dissolved in complete growth medium to achieve final concentrations of 3.7×10^{-10} M LF and 2.8×10^{-9} M PA. Assay plates were incubated at 37 °C, 5% CO$_2$, for 20 h and then removed from the incubator, de-lidded, and allowed to cool to room temperature for 1 h. Twenty microliters of ATPlite reagent (Perkin-Elmer) was added to each well. Luminescence values were then measured with the Victor^3 V reader (Perkin-Elmer).

MEK2 Cleavage Assay. MEK2 cleavage assay was performed as described previously with minimal modification (28). Briefly, six-well plates were seeded with 2×10^6 RAW 264.7 cells per well and allowed to grow overnight. Cells were then treated with 231 ng/mL PA and 33 ng/mL LF in the presence or absence of compound at 37 °C for ~2.5 h, washed with cold PBS, and lysed with MCF-7 lysis buffer supplemented with a complete mini protease inhibitor tablet (Roche). Ten micrograms of each protein sample was

subjected to SDS/PAGE and immunoblotting with anti–N-terminal MEK-2 antibody, HRP-conjugated anti-mouse HRP secondary antibody, and detected by Immun-Star HRP detection reagent (Bio-Rad).

Caspase-1 Activation. BMDMs from mice expressing transgenic for the LT-sensitive 129S1 allele of *Nlrp1b* were isolated and cultured as previously described (25). Briefly, femur exudates from two C57BL/6 or two C57BL/6$^{Nlrp1b(129S1)}$ transgenic animals were cultured for 7 d in DMEM (Cellgro, Mediatech, Inc.) supplemented with 10% (vol/vol) FBS (Atlanta Biologicals), 1% penicillin/streptomycin/glutamine (PSG; Gibco), and 2% (vol/vol) 14–22 conditioned media and incubated in a 5% CO$_2$ humidified incubator at 37 °C. Twenty thousand BMDMs from each of the four animals were plated in DMEM supplemented with 10% (vol/vol) FBS and 1% PSG. The following day, cells were treated with 20 μM EGA for 1 h before addition of LT for a further 2 h. FLICA reagent (Immunochemistry Technologies) was added for 1 h and then nuclei were stained with Hoechst 33342. Plates were imaged using an ImageXpress^{micro} automated high content screening system (Molecular Devices), and images were analyzed with MetaXpress software (Molecular Devices).

PA Pore Formation. Six-well plates were seeded with 1.8×10^6 RAW 264.7 cells per well and allowed to grow overnight. Cells were preincubated with EGA at indicated concentrations for 1 h before PA binding (400 ng/mL) for 1 h at 37 °C, at which time samples were washed with cold PBS and harvested as described previously. Protein samples were subjected to SDS/PAGE and immunoblotting with anti-PA serum and HRP-conjugated anti-rabbit secondary antibody.

Treatment with Bacterial Toxins. RAW264.7 cells or BMDMs were preincubated with EGA or derivatives for 1 h followed by intoxication with LT as indicated in figure legends. ATPlite viability reagent (Perkin-Elmer) was added, and relative luminescence was measured as above. For other toxins, HeLa cells were plated at 1×10^3 cells per well on each well of a 384-well plate (Greiner). The following day, EGA (Chembridge), NH$_4$Cl (Sigma-Aldrich), or bafilomycin A1 (Calbiochem) was added to the indicated concentrations and incubated for 1 h at 37 °C. DT was added to a concentration of 5 ng/mL, and ExoA and ricin were added at the indicated concentrations. Cells were incubated for 2 d, and 20 μL of ATPlite were added. Luminescence was measured using the Victor^{3}V (Perkin-Elmer).

Cell-cycle arrest induced by CDT was measured by propidium iodide staining and flow cytometry as previously described (43). To monitor subcellular localization of Ec-CdtB or Hd-CdtB, cells were stained and imaged as described (42) with the addition of mouse monoclonal anti-EEA1 antibody (1:50 dilution; Abcam). For each cell, images were collected from an average of 30 z-planes, each at a thickness of 0.2 μm. EEA1-localization analysis was conducted by using the DeltaVision SoftWoRx 3.5.1 software suite.

Viral Infections. For transductions with VSV-G and NiV glycoprotein pseudotyped lentiviral vectors or amphotropic and VSV-G pseudotyped MLV vectors, 6.5×10^4 cells/mL were seeded in DMEM onto 24-well plates. The following day, the media were removed, and fresh media containing EGA at indicated concentrations or DMSO only were added to cells. Dilutions of pseudotyped viral vectors encoding GFP were added 1 h later with 8 μg/mL polybrene. Cells were incubated overnight, and then virus and drug were removed, followed by another overnight incubation. Cells were then fixed in formaldehyde and analyzed by flow cytometry.

For LCMV infections, plates were seeded at 4×10^5 Vero cells/mL and incubated overnight at 37 °C. The next day, media were removed, and cells were infected in triplicate with 10^{-3}, 10^{-4}, and 10^{-5} dilution with a trisegmented LCMV Armstrong strain encoding GFP in the presence or absence of 20 μM EGA. The initial stock of LCMV-GFP was 7.3×10^6 pfu/mL. Cells and virus were incubated at 37 °C for 1 h, with shaking every 10 min. Virus media were removed, and 3 mL new media with or without EGA was added. Cells were incubated at 37 °C overnight. The next day, media were removed, and cells were trypsinized, centrifuged, and resuspended in 400 μL 1% paraformaldehyde to fix for 15 min in the dark. GFP expression was measured by flow cytometry.

Influenza infection was assessed using HeLa cells transfected with a Flu gLuc reporter construct, which expresses antisense transcripts of *Gaussia* luciferase flanked by the untranslated region of the influenza A/WSN/33 virus PA segment. Therefore, luciferase protein expression is dependent on the presence of the influenza virus polymerase complex, thus allowing quantification of viral infection. At 12 h post-transfection of the reporter construct, cells were infected with influenza A/WSN/33 virus at a multiplicity of infection of 0.5. Cells were treated with EGA at indicated concentrations

1 h before, simultaneous to, or 1 h after infection with virus. Culture supernatants were collected 10 h post-infection. *Gaussia* luciferase activity was determined using the Renilla Luciferase Assay System (Promega), and luminescence was measured using the Infinite M1000 plate reader (TECAN).

Lysotracker Red DND-99. HeLa cells were treated with EGA, NH$_4$Cl, or DMSO for 25 min at 37 °C and then stained with Lysotracker Red and Hoechst for 10 min at 37 °C. Cells were then washed, overlayed with PBS + 2% (vol/vol) FBS, and imaged by automated fluorescence microscopy (Image-Xpress^{micro}, Molecular Devices). Images were scored for number of Lysotracker Red-positive endosomes per cell using the granularity calculation module in MetaXpress software (Molecular Devices). An average of 175 cells per replicate was analyzed, and a minimum of three independent experiments, each performed in triplicate, were run.

EGFR Stability Assays. HeLa cells were seeded at 4×10^5 cells per well in a six-well plate; cultured overnight; serum-starved for 18 h; treated with DMSO, 20 μM EGA, or 10 mM NH$_4$Cl for 15 min at 37 °C; and then stimulated with serum-free medium containing the compounds and 100 ng/mL EGF (Gibco) for the indicated time periods. Cells were then washed with cold PBS and lysed in Nonidet P-40 lysis buffer (150 mM NaCl, 50 mM Tris, pH 8.0, 1% Nonidet P-40), and lysates were analyzed by immunoblotting with anti-EGFR 1:2,000 (Santa Cruz, #SC-03), anti-tubulin 1:5,000 (Sigma Aldrich, #T6074-200 μL), anti–p-ERK1/2 pY204 1:1,500 (Epitomics, #2219–1), and anti-ERK1/2 1:5,000 (BD, #610123). Blots were imaged using a Li-Cor Odyssey scanner.

For immunofluorescence microscopy, EGF-Alexa Fluor 647 (Invitrogen, #E35351), anti-EEA1 (BD Transduction Laboratories, #610456), and goat–anti-mouse Alexa Fluor 647 (Invitrogen, #A21245) were used. Glass-bottom 35-mm tissue culture plates (MatTek) were seeded with 4×10^5 cells. The cells were serum-starved overnight and incubated in medium containing 20 ng/mL EGF-Alexa Flour-647 and 20 μM EGA or DMSO on ice for 2 h. They were then chased for 60 min at 37 °C in serum-free medium containing only the compounds and fixed in 4% paraformaldehyde, permeabilized in 0.1% Triton-X-100 detergent, quenched in 50 mM NH$_4$Cl, and blocked in 10% (vol/vol) goat serum (Gibco). Images were acquired on a laser scanning confocal microscope (Axiovert 200M, Carl Zeiss LSM 5 Pascal) with a plan/neofluar 100× oil lens, N.A. 1.3. LSM 5 Pascal software (release version 4.2 sp1) was used to process the images.

Transferrin Recycling Assay. HeLa cells (3×10^5 cells per well) were seeded in triplicate on six-well plates. The cells were serum-starved overnight. Following a 15-min pretreatment with 20 μM EGA or DMSO, cells were stimulated with Tf conjugated to Alexa Fluor-488 (Tf-488) (Invitrogen) at 20 ng/mL for 5 min, washed with cold medium, and stripped twice with 0.2 M sodium acetate buffer (pH 4.5). The cells were rinsed in cold serum-free medium and excess unlabeled Tf and chased at 37 °C for the indicated amounts of time. Following the chase, the cells were stripped twice in the sodium acetate buffer. Tf-488 fluorescence from acid washes and medium was measured on a Wallac 1420 multilabel counter (PerkinElmer) at a 490/520-nm absorption/emission.

Phagocytosis Studies. THP-1 cells were added (1.5×10^5 cells/cm^2) to poly-L-lysine–coated (Sigma-Aldrich) glass coverslips in 2-cm^2 tissue culture wells, differentiated with phorbol 12-myristate 13-acetate (PMA, 100 nM) in RPMI-1640 with 10% (vol/vol) heat-inactivated FBS (HI-FBS) for 3 d at 37 °C in 5% CO$_2$, and pretreated for 1 h with 250 nm bafilomycin A, 20 μM EGA, or DMSO before addition of bacteria or latex beads. GFP-expressing *F. tularensis* LVS and escape incompetent GFP-LVS-ΔIglC were prepared and cultured as previously described (63–65) and added to monolayers of THP-1 cells on glass

coverslips in 24-well plates. The plates were centrifuged at $800 \times g$ for 30 min 4 °C, incubated at 37 °C for 30 min, washed three times with HBSS to remove nonadherent bacteria, and incubated for 3 h at 37 °C in fresh RPMI-1640 with 10% (vol/vol) HI-FBS containing 20 μM EGA, 250 nm bafilomycin, or DMSO vehicle. Phagosome integrity was assessed by a modification of the differential digitonin permeabilization method of Checroun et al. (33), which permeabilizes the plasma membrane but not phagosomal membranes. Briefly, monolayers were fixed for exactly 1 min with HBSS + 4% (vol/vol) paraformaldehyde followed by permeabilization for exactly 1 min with 0.05 mg/mL digitonin in KHM (110 mM potassium acetate, 20 mM Hepes, pH 7.3, 2 mM MgCl2) with 6% (vol/vol) sucrose, washed twice with KHM containing 6% sucrose, and incubated with rabbit anti-*F. tularensis* antibody (1:1,000 dilution; Becton Dickinson) in KHM buffer containing 6% sucrose and 0.1% BSA, washed three times with KHM containing 6% sucrose, fixed for 30 min in 4% paraformaldehyde in 75 mM sodium phosphate (pH 7.4), permeabilized in 0.1% saponin in PBS, washed with PBS, and incubated with Texas Red-X conjugated goat anti-rabbit IgG (Invitrogen) for 90 min at room temperature. Monolayers were washed, incubated with DAPI (1 μg/mL), mounted with Prolong Gold anti-fade mounting medium, and viewed by phase and fluorescence microscopy. Green fluorescent bacteria that stain red were scored as having permeabilzed their phagosomes. Escape incompetent GFP-LVS-ΔIglC are inaccessible to antibody after digitonin permeabilization of the plasma membrane and serve as negative controls. At least 400 cells were examined and enumerated in duplicate wells, and the experiments were conducted twice with similar results. Numbers of GFP bacteria per DAPI nucleus under each of the conditions was determined by particle analysis using ImageJ software.

To evaluate the impact of inhibitors on fusion of latex bead phagosomes with secondary lysosomes, we labeled the lysosomal compartments of PMA-differentiated THP-1 cells with lysine-fixable Texas Red-Dextran (70 kDa, 0.05 mg/mL; Invitrogen) for 12 h. Macrophages were treated with 250 nM bafilomycin A, 20 μM EGA, or DMSO vehicle control for 30 min before uptake of latex beads. Fluorescent blue 1-μm polystyrene microbeads (2.5% solids; Polysciences) were opsonized with human AB serum (66), diluted 50,000-fold (10^6 particles/mL) in RPMI-1640 with 10% HI-FBS, and added to the monolayers of differentiated THP-1 cells in 24-well plates. After incubation for 3 h at 37 °C with vehicle or inhibitors, the macrophages were fixed, stained with DAPI, and mounted as described above. Colocalization of latex beads with Texas Red Dextran fluorescence was assessed by fluorescence and phase-contrast microscopy. At least 40 particles were examined on duplicate coverslips, and the experiments were repeated twice with similar results.

Statistical Analysis. Data were analyzed using GraphPad Prism5 software. Group size, number of replicates, and specific statistical methods used are presented for each experiment in the figure legends.

1. Knodler LA, Celli J, Finlay BB (2001) Pathogenic trickery: Deception of host cell processes. *Nat Rev Mol Cell Biol* 2(8):578–588.

2. Sandvig K, van Deurs B (2005) Delivery into cells: Lessons learned from plant and bacterial toxins. *Gene Ther* 12(11):865–872.

3. Saenz JB, Doggett TA, Haslam DB (2007) Identification and characterization of small molecules that inhibit intracellular toxin transport. *Infect Immun* 75(9):4552–4561.

4. Wahome PG, Bai Y, Neal LM, Robertus JD, Mantis NJ (2010) Identification of small-molecule inhibitors of ricin and shiga toxin using a cell-based high-throughput screen. *Toxicon* 56(3):313–323.

5. Stechmann B, et al. (2010) Inhibition of retrograde transport protects mice from lethal ricin challenge. *Cell* 141(2):231–242.

6. Duesbery NS, et al. (1998) Proteolytic inactivation of MAP-kinase-kinase by anthrax lethal factor. *Science* 280(5364):734–737.

7. Vitale G, et al. (1999) Anthrax lethal factor cleaves the N-terminus of MAPKKS and induces tyrosine/threonine phosphorylation of MAPKS in cultured macrophages. *J Appl Microbiol* 87(2):288.

8. Levinsohn JL, et al. (2012) Anthrax lethal factor cleavage of Nlrp1 is required for activation of the inflammasome. *PLoS Pathog* 8(3):e1002638.

9. Hellmich KA, et al. (2012) Anthrax lethal factor cleaves mouse nlrp1b in both toxin-sensitive and toxin-resistant macrophages. *PLoS ONE* 7(11):e49741.

10. Chavarría-Smith J, Vance RE (2013) Direct proteolytic cleavage of NLRP1B is necessary and sufficient for inflammasome activation by anthrax lethal factor. *PLoS Pathog* 9(6):e1003452.

11. Moayeri M, Leppla SH (2009) Cellular and systemic effects of anthrax lethal and edema toxin. *Mol Aspects Med* 30(6):439–455.

12. Beall FA, Taylor MJ, Thorne CB (1962) Rapid lethal effect in rats of a third component found upon fractionating the toxin of Bacillus anthracis. *J Bacteriol* 83:1274–1280.

13. Milne JC, Furlong D, Hanna PC, Wall JS, Collier RJ (1994) Anthrax protective antigen forms oligomers during intoxication of mammalian cells. *J Biol Chem* 269(32):20607–20612.

14. Mogridge J, Cunningham K, Lacy DB, Mourez M, Collier RJ (2002) The lethal and edema factors of anthrax toxin bind only to oligomeric forms of the protective antigen. *Proc Natl Acad Sci USA* 99(10):7045–7048.

15. Kintzer AF, et al. (2009) The protective antigen component of anthrax toxin forms functional octameric complexes. *J Mol Biol* 392(3):614–629.
16. Bradley KA, Mogridge J, Mourez M, Collier RJ, Young JA (2001) Identification of the cellular receptor for anthrax toxin. *Nature* 414(6860):225–229.
17. Scobie HM, Rainey GJ, Bradley KA, Young JA (2003) Human capillary morphogenesis protein 2 functions as an anthrax toxin receptor. *Proc Natl Acad Sci USA* 100(9): 5170–5174.
18. Koehler TM, Collier RJ (1991) Anthrax toxin protective antigen: Low-pH-induced hydrophobicity and channel formation in liposomes. *Mol Microbiol* 5(6):1501–1506.
19. Milne JC, Collier RJ (1993) pH-dependent permeabilization of the plasma membrane of mammalian cells by anthrax protective antigen. *Mol Microbiol* 10(3):647–653.
20. Miller CJ, Elliott JL, Collier RJ (1999) Anthrax protective antigen: Prepore-to-pore conversion. *Biochemistry* 38(32):10432–10441.
21. Abrami L, Lindsay M, Parton RG, Leppla SH, van der Goot FG (2004) Membrane insertion of anthrax protective antigen and cytoplasmic delivery of lethal factor occur at different stages of the endocytic pathway. *J Cell Biol* 166(5):645–651.
22. Boyden ED, Dietrich WF (2006) Nalp1b controls mouse macrophage susceptibility to anthrax lethal toxin. *Nat Genet* 38(2):240–244.
23. Wickliffe KE, Leppla SH, Moayeri M (2008) Anthrax lethal toxin-induced inflammasome formation and caspase-1 activation are late events dependent on ion fluxes and the proteasome. *Cell Microbiol* 10(2):332–343.
24. Squires RC, Muehlbauer SM, Brojatsch J (2007) Proteasomes control caspase-1 activation in anthrax lethal toxin-mediated cell killing. *J Biol Chem* 282(47):34260–34267.
25. Averette KM, et al. (2009) Anthrax lethal toxin induced lysosomal membrane permeabilization and cytosolic cathepsin release is Nlrp1b/Nalp1b-dependent. *PLoS ONE* 4(11):e7913.
26. Milne JC, Blanke SR, Hanna PC, Collier RJ (1995) Protective antigen-binding domain of anthrax lethal factor mediates translocation of a heterologous protein fused to its amino- or carboxy-terminus. *Mol Microbiol* 15(4):661–666.
27. Friedlander AM (1986) Macrophages are sensitive to anthrax lethal toxin through an acid-dependent process. *J Biol Chem* 261(16):7123–7126.
28. Sanchez AM, et al. (2007) Amiodarone and bepridil inhibit anthrax toxin entry into host cells. *Antimicrob Agents Chemother* 51(7):2403–2411.
29. Sigismund S, et al. (2008) Clathrin-mediated internalization is essential for sustained EGFR signaling but dispensable for degradation. *Dev Cell* 15(2):209–219.
30. Carpenter G, Cohen S (1976) 125I-labeled human epidermal growth factor. Binding, internalization, and degradation in human fibroblasts. *J Cell Biol* 71(1):159–171.
31. Chong A, et al. (2008) The early phagosomal stage of Francisella tularensis determines optimal phagosomal escape and Francisella pathogenicity island protein expression. *Infect Immun* 76(12):5488–5499.
32. Chong A, et al. (2012) Cytosolic clearance of replication-deficient mutants reveals Francisella tularensis interactions with the autophagic pathway. *Autophagy* 8(9): 1342–1356.
33. Checroun C, Wehrly TD, Fischer ER, Hayes SF, Celli J (2006) Autophagy-mediated reentry of Francisella tularensis into the endocytic compartment after cytoplasmic replication. *Proc Natl Acad Sci USA* 103(39):14578–14583.
34. Schlierf B, Fey GH, Hauber J, Hocke GM, Rosorius O (2000) Rab11b is essential for recycling of transferrin to the plasma membrane. *Exp Cell Res* 259(1):257–265.
35. Collier RJ (2001) Understanding the mode of action of diphtheria toxin: A perspective on progress during the 20th century. *Toxicon* 39(11):1793–1803.
36. Iglewski BH, Kabat D (1975) NAD-dependent inhibition of protein synthesis by Pseudomonas aeruginosa toxin. *Proc Natl Acad Sci USA* 72(6):2284–2288.
37. Taupiac MP, Alami M, Beaumelle B (1996) Translocation of full-length Pseudomonas exotoxin from endosomes is driven by ATP hydrolysis but requires prior exposure to acidic pH. *J Biol Chem* 271(42):26170–26173.
38. Sandvig K, Olsnes S (1980) Diphtheria toxin entry into cells is facilitated by low pH. *J Cell Biol* 87(3 Pt 1):828–832.
39. Gargi A, Reno M, Blanke SR (2012) Bacterial toxin modulation of the eukaryotic cell cycle: Are all cytolethal distending toxins created equally? *Front Cell Infect Microbiol* 2:124.
40. Lara-Tejero M, Galán JE (2000) A bacterial toxin that controls cell cycle progression as a deoxyribonuclease I-like protein. *Science* 290(5490):354–357.
41. Guerra L, Cortes-Bratti X, Guidi R, Frisan T (2011) The biology of the cytolethal distending toxins. *Toxins (Basel)* 3(3):172–190.
42. Gargi A, et al. (2013) Cellular interactions of the cytolethal distending toxins from Escherichia coli and Haemophilus ducreyi. *J Biol Chem* 288(11):7492–7505.
43. Eshraghi A, et al. (2010) Cytolethal distending toxin family members are differentially affected by alterations in host glycans and membrane cholesterol. *J Biol Chem* 285(24):18199–18207.
44. Carette JE, et al. (2011) Global gene disruption in human cells to assign genes to phenotypes by deep sequencing. *Nat Biotechnol* 29(6):542–546.
45. White J, Matlin K, Helenius A (1981) Cell fusion by Semliki Forest, influenza, and vesicular stomatitis viruses. *J Cell Biol* 89(3):674–679.
46. Borrow P, Oldstone MB (1994) Mechanism of lymphocytic choriomeningitis virus entry into cells. *Virology* 198(1):1–9.
47. Di Simone C, Zandonatti MA, Buchmeier MJ (1994) Acidic pH triggers LCMV membrane fusion activity and conformational change in the glycoprotein spike. *Virology* 198(2):455–465.
48. McClure MO, Sommerfelt MA, Marsh M, Weiss RA (1990) The pH independence of mammalian retrovirus infection. *J Gen Virol* 71(Pt 4):767–773.
49. Diederich S, Thiel L, Maisner A (2008) Role of endocytosis and cathepsin-mediated activation in Nipah virus entry. *Virology* 375(2):391–400.
50. Emonet SF, Garidou L, McGavern DB, de la Torre JC (2009) Generation of recombinant lymphocytic choriomeningitis viruses with trisegmented genomes stably expressing two additional genes of interest. *Proc Natl Acad Sci USA* 106(9):3473–3478.
51. Lee AM, Pasquato A, Kunz S (2011) Novel approaches in anti-arenaviral drug development. *Virology* 411(2):163–169.
52. Service RF (1997) Researchers seek new weapon against the flu. *Science* 275(5301): 756–757.
53. Géssner A, Lother H (1989) Homologous interference of lymphocytic choriomeningitis virus involves a ribavirin-susceptible block in virus replication. *J Virol* 63(4):1827–1832.
54. Sidwell RW, et al. (1972) Broad-spectrum antiviral activity of Virazole: 1-Beta-D-ribofuranosyl-1,2,4-triazole-3-carboxamide. *Science* 177(4050):705–706.
55. Terra JK, et al. (2010) Cutting edge: Resistance to Bacillus anthracis infection mediated by a lethal toxin sensitive allele of Nalp1b/Nlrp1b. *J Immunol* 184(1):17–20.
56. Macia E, et al. (2006) Dynasore, a cell-permeable inhibitor of dynamin. *Dev Cell* 10(6): 839–850.
57. von Kleist L, et al. (2011) Role of the clathrin terminal domain in regulating coated pit dynamics revealed by small molecule inhibition. *Cell* 146(3):471–484.
58. Klausner RD, Donaldson JG, Lippincott-Schwartz J (1992) Brefeldin A: Insights into the control of membrane traffic and organelle structure. *J Cell Biol* 116(5):1071–1080.
59. Cortese K, et al. (2013) The HSP90 inhibitor geldanamycin perturbs endosomal structure and drives recycling ErbB2 and transferrin to modified MVBs/lysosomal compartments. *Mol Biol Cell* 24(2):129–144.
60. Engel S, et al. (2011) Role of endosomes in simian virus 40 entry and infection. *J Virol* 85(9):4198–4211.
61. Stenmark H, et al. (1994) Inhibition of rab5 GTPase activity stimulates membrane fusion in endocytosis. *EMBO J* 13(6):1287–1296.
62. Yogeeswari P, et al. (2005) Discovery of N-(2,6-dimethylphenyl)-substituted semicarbazones as anticonvulsants: Hybrid pharmacophore-based design. *J Med Chem* 48(20):6202–6211.
63. Clemens DL, Horwitz MA (2007) Uptake and intracellular fate of Francisella tularensis in human macrophages. *Ann N Y Acad Sci* 1105:160–186.
64. Clemens DL, Lee BY, Horwitz MA (2012) O-antigen-deficient Francisella tularensis Live Vaccine Strain mutants are ingested via an aberrant form of looping phagocytosis and show altered kinetics of intracellular trafficking in human macrophages. *Infect Immun* 80(3):952–967.
65. Clemens DL, Lee BY, Horwitz MA (2009) Francisella tularensis phagosomal escape does not require acidification of the phagosome. *Infect Immun* 77(5):1757–1773.
66. Horwitz MA (1984) Phagocytosis of the Legionnaires' disease bacterium (Legionella pneumophila) occurs by a novel mechanism: Engulfment within a pseudopod coil. *Cell* 36(1):27–33.